Online-Journals.org

iJOE International Journal of Online and Biomedical Engineering

iJOE | eISSN: 2626-8493 | Vol. 22 No. 5 (2026) | OPEN ACCESS

https://doi.org/10.3991/ijoe.v22i05.59611

PAPER

Algorithm-Based Optimization of Taylor Spatial Frame Adjustments for Improved Tibial Deformity Correction

Tao Liu[1,2], Xiaolong Qi[1,2](✉), Yonghua Lu[3], Xinyu Di[3], Yu Zhang[4]

[1]Yili Normal University, Yining, China

[2]Yili Key Laboratory of Intelligent Computing Research and Application, Yining, China

[3]Nanjing University of Aeronautics and Astronautics, Nanjing, China

[4]Jiangsu Province Hospital, Nanjing, China

qixl@ylnu.edu.cn

ABSTRACT

The Taylor spatial frame (TSF) provides minimal surgical trauma during installation, convenient adjustment, and the ability to perform multi-plane correction simultaneously. These advantages have led to its widespread adoption in trauma orthopedics and reconstruction. In conventional TSF-assisted correction, the non-linear coupling between the six struts often causes unintended platform deviations, leading to bone–tissue collision and patient discomfort. This study proposes an algorithmic optimization method combining multi-objective genetic algorithm (MOGA) and ant colony optimization (ACO) to reduce such deviations and improve correction precision. The TSF correction process integrates intelligent algorithms with a specially designed fitness function to optimize the correction plan. Experimental results show that the proposed method effectively reduces TSF deviations during the correction process. This reduction minimizes the risk of bone collisions with surrounding tissues and alleviates patient pain during the procedure. The method's clinical value was further validated by aiding the treatment process in a tibial deformity correction case. The proposed method enhanced the linearity of TSF movement, thereby alleviating patient discomfort during the correction process. This approach shows promising potential for TSF clinical treatment.

KEYWORDS

intelligent algorithms, kinematics analysis, tibial deformity correction, Taylor spatial frame (TSF)

1 INTRODUCTION

Orthopedic surgical fixation methods are divided into internal and external approaches. Internal fixation uses rigid metallic devices placed inside the body to stabilize fracture segments. In contrast, external fixation technology employs transcutaneous pins to connect the bone segments to an external fixator.

Liu, T., Qi, X., Lu, Y., Di, X., Zhang, Y. (2026). Algorithm-Based Optimization of Taylor Spatial Frame Adjustments for Improved Tibial Deformity Correction. *International Journal of Online and Biomedical Engineering (iJOE)*, 22(5), pp. 109–123. https://doi.org/10.3991/ijoe.v22i05.59611

Article submitted 2025-11-12. Revision uploaded 2026-02-03. Final acceptance 2026-02-03.

The external fixator establishes a stable connection between the two ends of the bone, allowing adjustments to move the bone segments into the desired position. This approach provides excellent stability and a favorable biomechanical environment for bone healing. The development of external fixation technology reached a milestone with G.A. Ilizarov's invention of the Ilizarov frame and his validation of distraction osteogenesis. This innovation expanded the application of external fixation beyond fracture treatment to include limb deformity correction and defect repair. With the widespread use and promotion of the Ilizarov frame, several limitations have also been exposed, such as the inability to correct multi-plane deformities within a short time frame and its relatively weak structural stability [1–3]. Based on the Ilizarov frame, J. Charles Taylor and Harold S. Taylor applied Stewart platform technology to invent the Taylor spatial frame (TSF). With the assistance of computer technology, the TSF has become a representative tool in digital orthopedic surgery.

Compared to traditional frames, the TSF allows for simultaneous adjustment of both angles and distances in three-dimensional space within a single correction period, avoiding the tedious process of multiple structural adjustments required by traditional frames when correcting multi-plane deformities [4]. The spatial rings and struts of the TSF form multiple stable triangular structures, and its overall design is similar to the octahedral structure of a diamond crystal. Compared to the equidiameter Ilizarov frame, the TSF offers advantages in axial strength, bending strength, and torsional strength [5]. To accommodate different installation sites and adapt to various correction scenarios, the TSF has evolved into several configurations. Although the shapes differ, its operation can be summarized as follows: by adjusting the geometric dimensions of a specific component, the positional relationship between the two platforms of the external fixator is altered, thereby achieving the goal of mobilizing the bone segments through traction [6]. Due to its advantages, such as minimal surgical trauma, convenient adjustment, and the ability to perform multi-plane correction, the TSF has been gradually applied in fields such as trauma orthopedics, reconstructive surgery, and pediatric orthopedics [7]. However, despite these advantages, clinical use of TSF still faces challenges of motion accuracy. Small calculation or adjustment errors can lead to spatial deviation between the proximal and distal rings, forcing irregular movement paths during distraction. These deviations may cause bone collision or excessive soft-tissue tension, affecting patient recovery. Therefore, reducing the deviation of the TSF moving platform is a key problem needing investigation.

Starr et al. [8] conducted a study on the follow-up measurement process in TSF correction surgeries. They combined time-lapse computed tomography with volume fusion techniques to construct three-dimensional models for monitoring tibial deformity correction. Liu et al. [9] applied computer-assisted 3D reconstruction and reduction trajectory planning using Mimics software to perform virtual fracture reduction and deformity correction. They first imported the 3D model into SolidWorks software. The electronic prescriptions derived from the length changes of the six struts were calculated by SolidWorks. Fracture reduction was conducted by adjusting the lengths of the six struts according to the electronic prescription. These studies primarily focused on using computer technology to observe the correction process of TSF without optimizing the adjustment method.

To address the above clinical issues, this paper introduces a computer-assisted correction planning method integrating TSF kinematic modeling with multi-objective

genetic algorithm (MOGA) and ant colony optimization (ACO) algorithms, aiming to minimize platform deviation and enhance the precision and safety of the correction process. The correction process of a clinical tibial deformity case was assisted by the proposed method. This paper established a model with equal dimensions based on the results of the osteotomy and frame installation surgeries. Simulation experiments demonstrated the feasibility and effectiveness of the correction method. This paper provided prescription recommendations by reserving space for bone growth and dynamically updating the electronic prescription based on follow-up results. Ten months post-surgery, the patient's proximal and distal tibial ends were connected, and the deformity was eliminated.

2 METHODS

2.1 Calculation principles of TSF kinematics

The TSF consists of two platforms—a static platform (proximal ring attached to the reference bone segment) and a moving platform (the distal ring connected to the mobile bone segment). During correction, maintaining the ideal movement trajectory of the distal ring is critical for avoiding bone collision and ensuring precise alignment. A Cartesian coordinate system is established on the static platform, with its origin at the platform's center. The *x*-axis passes through the midpoint of the spatial ring's short edge, the *y*-axis passes through the midpoint of the long edge, and the *z*-axis is perpendicular to the plane of the spatial ring, as shown in Figure 1.

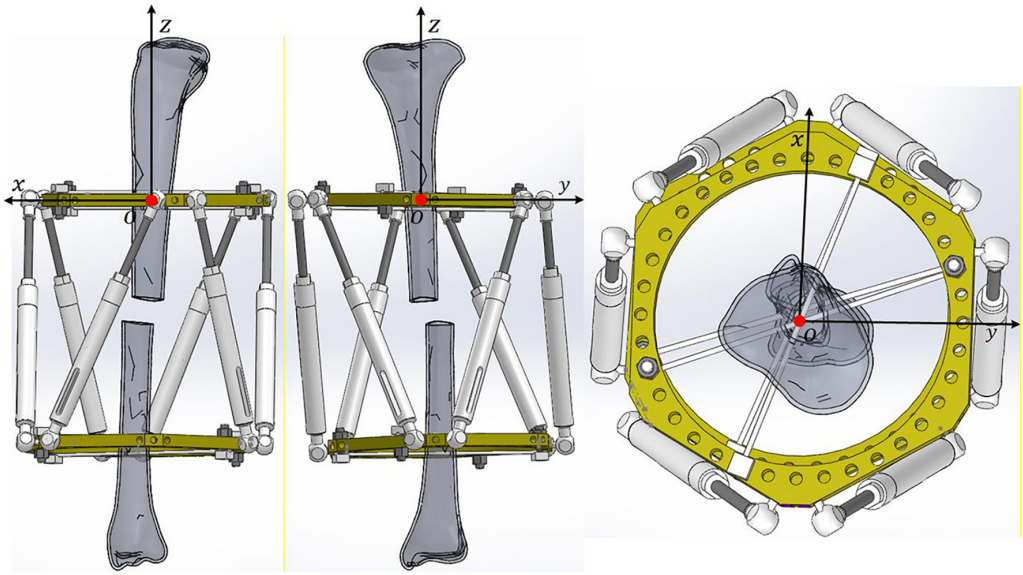

Fig. 1. Establishment of coordinate system

The spatial relationship between the proximal (reference) and distal (moving) rings can be defined by six independent variables: three translational displacements (along the *x*-, *y*-, and *z*-axes) and three rotational angles (about these axes). Each strut connects predefined hinge points on both rings. Given the ring geometry and the spatial transformation matrix between the two coordinate systems,

the length of each strut L_i (i = 1, ..., 6) can be expressed as the Euclidean distance between the corresponding hinge points on the two rings:

$$L_i = \| R \cdot p_i + T - q_i \| \tag{1}$$

where R is the rotation matrix describing the orientation of the moving ring, T is its translation vector relative to the reference ring, p_i and q_i are the pivotal coordinates of the ith strut on the upper and lower rings, respectively.

This basic kinematic formulation represents the standard modeling principle of hexapod external fixators and serves as the mathematical foundation for the optimization algorithm developed in this study. To avoid redundancy, detailed derivations of these equations are omitted here but follow standard formulations established in prior TSF studies. The subsequent section 2.2 builds upon this framework to introduce the proposed algorithm for minimizing platform deviation and optimizing strut adjustment sequences.

2.2 Formulation of deformity correction plan

Planning of strut adjustment lengths. The relationship between TSF strut lengths and the moving platform's pose is non-linear [10], which can cause unintended deviations and soft tissue compression during traction. Unlike the common approach of uniform strut length changes, this study employs MOGA to optimize the adjustment plan. In this context, an individual represents a specific adjustment scheme, constrained by the adjustment range and step count.

A population of 20 individuals is randomly initialized. The fitness of each individual is evaluated to guide the selection of the optimal scheme. The process repeats for 5 iterations to ensure computational efficiency for clinical use while maintaining stable convergence.

In this study, the fitness function F is designed based on the motion offset of the moving platform. Taking ten adjustment steps during the correction process as an example, it is expressed as (2):

$$\begin{cases} D_{ij} = \left\| (d_{ij} - O') - \dfrac{(O'_1 - O')(O'_1 - O')^T}{(O'_1 - O')^T (O'_1 - O')} (d_{ij} - O') \right\| \\ F = \displaystyle\sum_{j=1}^{6} \sum_{i=1}^{10} e^{\frac{1}{D_{ij}}} \qquad i \in [1,10], \quad j \in [1,6] \end{cases} \tag{2}$$

In the equation, d_{ij} represents the coordinates of the intermediate point generated after the moving platform's pose changes; O' is the starting point of the moving platform's center, and O'_1 is the endpoint of the motion. D_{ij} is the distance from each intermediate point to the line segment $O'O'_1$. The fitness function F reflects the offset of the moving platform throughout the entire correction process. For the obtained strut length data, forward and inverse kinematics analyses are first used to derive the pose parameters of the moving platform. Based on these pose parameters, the center coordinates of the moving platform are calculated and then substituted into the fitness function to determine the individual's fitness value.

Planning the sequence of strut adjustments. Although the optimal length for each strut adjustment can be obtained using MOGA, the six struts of the TSF cannot be adjusted simultaneously, and different adjustment sequences result in varying poses of the moving platform. In the correction process, adjusting all six TSF struts, which makes up a single adjustment cycle, takes a significant amount of time and is not accomplished quickly. The common practice is to complete the adjustment process over the course of several days. This implies that if adjusting a specific strut causes a significant offset distance of the moving platform, the patient may experience prolonged discomfort. To minimize this risk, this study employs the ACO algorithm to plan the adjustment sequence of the struts, aiming to minimize the offset distance.

In this model, m ants are distributed across nodes representing the struts. The transition probability $p_{ij}^{k}(t)$, which governs the likelihood of an ant moving from strut i to strut j (scheme ij) at time t, is defined as:

$$p_{ij}^{k}(t)=\frac{[\tau_{ij}(t)]^{\alpha}\cdot[\eta_{ij}(t)]^{\beta}}{\sum_{j\in allow_{k}}[\tau_{ij}(t)]^{\alpha}\cdot[\eta_{ij}(t)]^{\beta}} \tag{3}$$

where $allow_k$ denotes the set of available struts not yet included in the tabu list. The heuristic factor $\eta_{ij} = 1/D_{ij}$ represents the desirability of the scheme, where D_{ij} is the platform deviation derived from the distance between the mobile platform center and the target axis. The hyperparameters α and β control the influence of pheromone intensity and heuristic guidance, respectively. In this study, α was set to 1 and β to 4 based on preliminary empirical tests to prioritize deviation reduction while maintaining search diversity.

As ants traverse the paths, the pheromone level τ_{ij} is updated to reflect the quality of the adjustment sequences:

$$\begin{cases}\tau_{ij}(t+1)=(1-\rho)\cdot\tau_{ij}(t)+\Delta\tau_{ij}(t)\\ \Delta\tau_{ij}(t)=\sum_{k=1}^{m}\Delta\tau_{ij}^{k}(t)\\ \Delta\tau_{ij}^{k}(t)=\dfrac{1}{L_{k}}\end{cases} \tag{4}$$

Here, the evaporation coefficient ρ was set to 0.2 to prevent premature convergence. $\Delta\tau_{ij}^{k}(t)$ is the pheromone deposited by the kth ant, and L_k represents the total offset distance generated by that ant's specific adjustment scheme. By iterating this process, the algorithm identifies the sequence with the minimum cumulative deviation.

The proposed MOGA-ACO integration was validated through a physical experiment using a fractured tibia model. After calculating the target strut lengths via inverse kinematics, the optimized adjustment plan was executed. A three-coordinate measuring arm was used to establish the spatial coordinate system and acquire the coordinates of the reference points. The experiment confirmed that the algorithmically planned sequence successfully achieved precise bone segment alignment, and the correction process is shown in Figure 2.

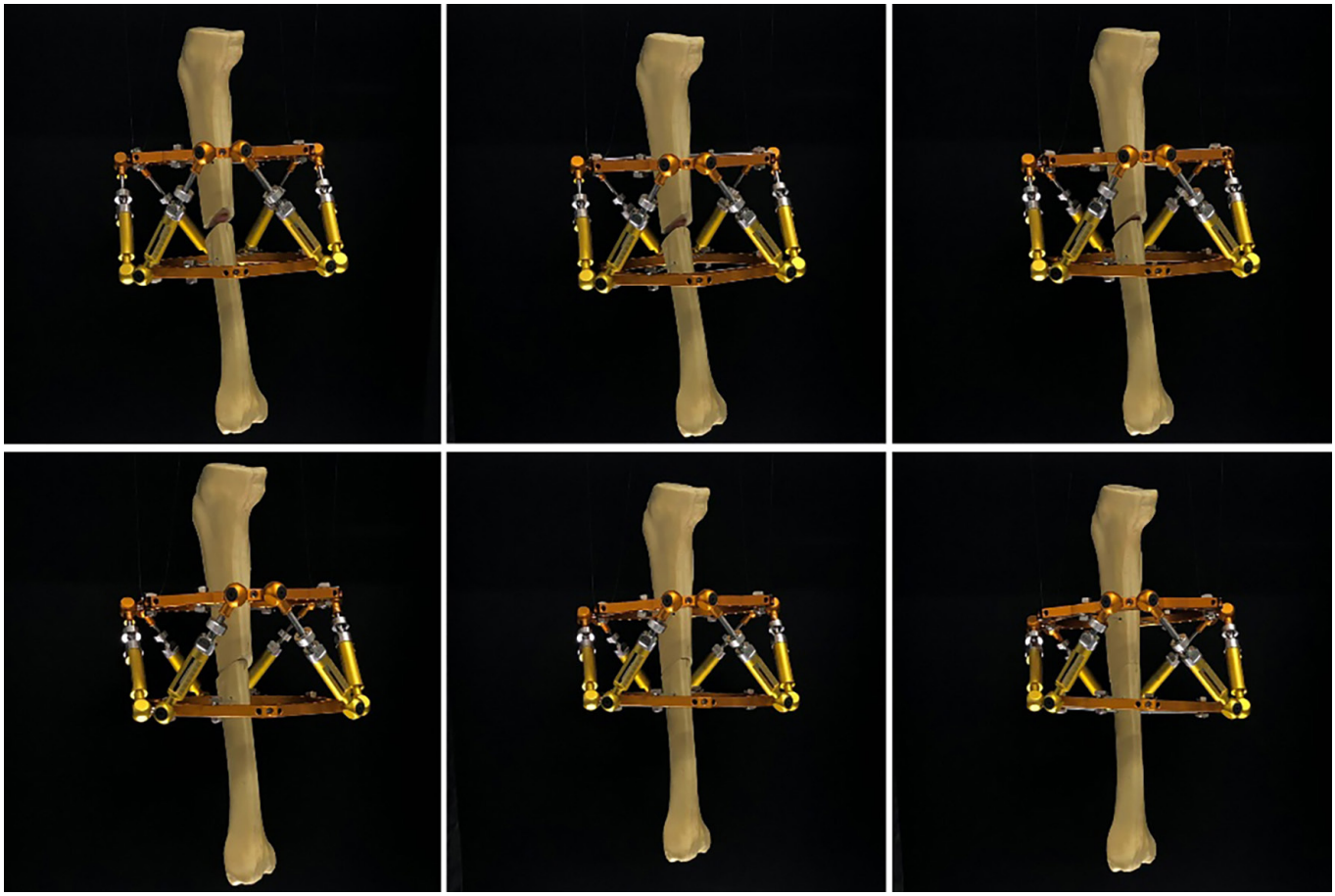

Fig. 2. Physical correction experiment process

3 EXPERIMENT AND RESULTS

Instead of a formal clinical trial, this study presents a clinical feasibility demonstration to evaluate how the proposed algorithm can assist surgeons in optimizing TSF adjustment plans for a specific case.

3.1 Clinical case

This paper focused on a clinical case of tibial deformity from Jiangsu Province Hospital, assisting in its correction process. The clinical treatment was conducted with the patient presenting a deformity at the proximal tibia, as shown in Figure 3. After the clinical doctor performed the TSF installation and osteotomy, our study provided assistance in the correction process and conducted regular follow-up observations to monitor the deformity correction. The effectiveness of the proposed method was validated based on 10 months of follow-up records.

Fig. 3. Preoperative X-ray of the patient

After observing the patient's deformity preoperatively, the first step was to perform the external fixator installation surgery, as shown in Figures 4a and b. The clinical doctors assessed the appropriate locations for the upper and lower rings. The affected limb was positioned at the center of the ring, and the entry points for the fixation pins were selected along the perpendicular line to the anatomical axis of the tibia. Doctors inserted fixation pins at both the distal and proximal ends to install the rings. Struts of appropriate size were selected to secure the external fixator between the two rings. To facilitate knee flexion, the proximal ring was designed as a 2/3 opening ring with the opening facing dorsally. After the installation of the fixator, the doctor performed a corrective osteotomy based on the deformity to ensure proper alignment of the bone axes. After the osteotomy and fixator installation, the patient's tibia X-rays were taken, shown in Figures 4c and d.

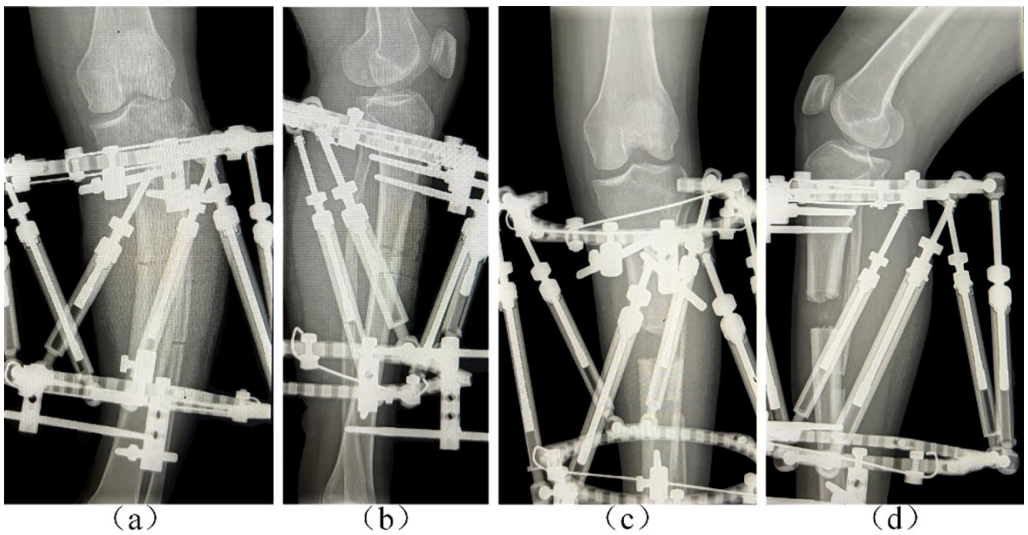

Fig. 4. Pre-correction X-ray images: (a) and (b) post-frame installation; (c) and (d) post-osteotomy

The deformity is characterized by antero-posterior displacement (APD), lateral displacement (LD), antero-posterior angulation (APA), lateral angulation (LA), axial plane angularity (APA_{ax}), and length (ALD_{ax}) as shown in Table 1.

Table 1. The deformity parameters of the affected limb before correction

Parameters	Values Before Correction
APD (mm)	18.25
LD (mm)	17.74
ALD_{ax} (mm)	61.93
APA (°)	10.33
LA (°)	5.38
APA_{ax} (°)	0

3.2 Simulation experiment of deformity correction

Based on the simulation experiment, the results of the osteotomy and the installation of the external fixator, an equal-dimension model was established with the struts numbered in different colors. The path planning method described earlier was used for simulation experiments to observe the correction effect, as shown in Figure 5.

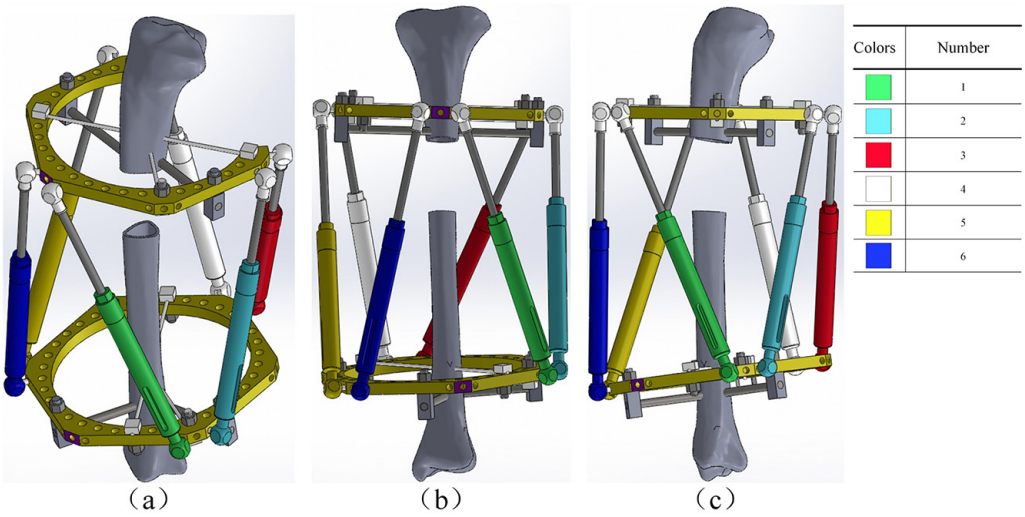

Fig. 5. Model established based on postoperative results: (a) overall view; (b) frontal view; (c) lateral view

In this study, the simulation step size was intentionally set larger than the clinical distraction rate to amplify observable deviation effects and evaluate the algorithm's sensitivity. Clinically, the distraction rate after osteotomy generally does not exceed 1.0 mm/day and is often approximately 0.7–0.8 mm/day for adult tibial cases. Increasing the adjustment magnitude only served to visualize the deviation trend more clearly, without altering the underlying physical relationship.

MOGA was used to plan the strut adjustment lengths to minimize the offset. Figure 6 shows the trajectory of the moving platform's center compared to the method of uniformly adjusting the strut lengths.

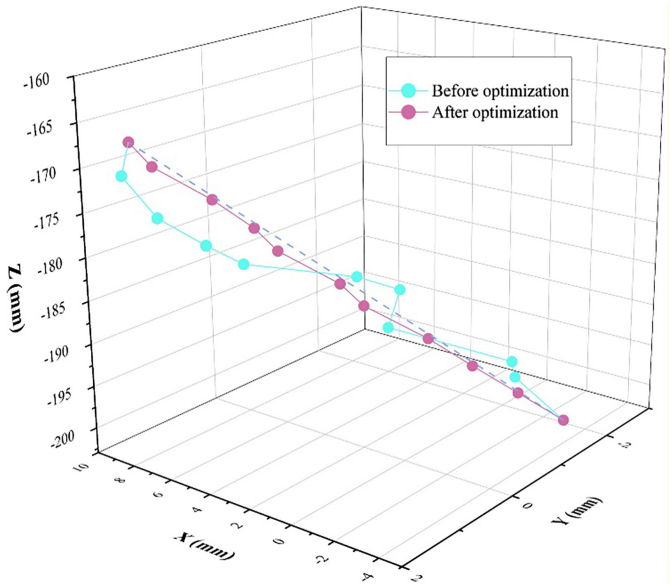

Fig. 6. Trajectory of the moving platform before and after strut adjustment length optimization

The offset distance of the moving platform is shown in Table 2. From Figure 6, it can be observed that after applying the strut length planning method, the intermediate points of the moving platform's movement are closer to the line connecting the starting and ending points. In contrast, before optimization, the moving platform's path formed multiple segments of a zigzag line, resulting in a larger offset distance.

Table 2. Comparison of offset distances before and after optimization of strut adjustment length planning

Number of Adjustments	Offset Distances (mm)	
	Before Optimization	After Optimization
1	1.2122	0.2119
2	0.6478	0.3264
3	2.3597	0.3026
4	1.6757	0.3873
5	0.6715	0.2651
6	1.6083	0.0775
7	0.9504	0.4989
8	0.9573	0.808
9	1.2291	1.0015
10	0	0
Mean	0.4858	0.2289
Variance	0.6194	0.2948

Using the method of evenly adjusting strut lengths, the total offset is 11.312 mm. Under the planning of the proposed method, both the total offset of the moving platform and the offset during each adjustment are significantly reduced. After optimization, the total offset is reduced to 3.8791 mm, a reduction of approximately 65.7%. Furthermore, the smaller values of mean and variance indicate a smoother movement of the platform.

After determining the optimal length for each adjustment, we applied the ACO algorithm to plan the adjustment sequence of the struts. Compared with adjusting the struts in numerical order, the movement trajectory of the platform is shown in Figure 7.

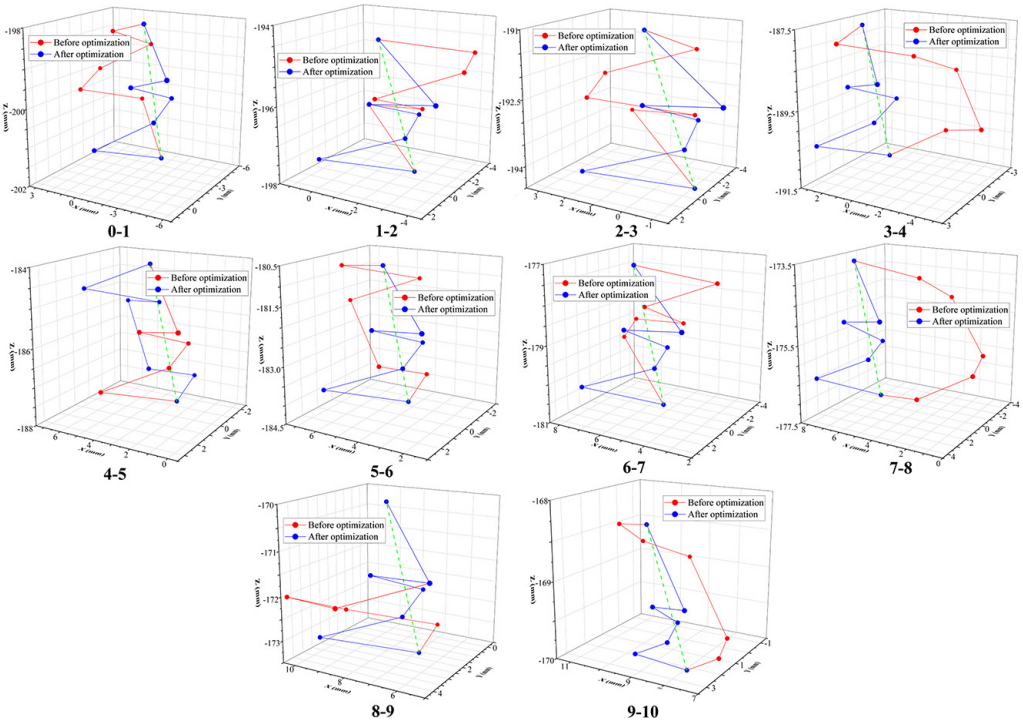

Fig. 7. Trajectory of the moving platform before and after planning the strut adjustment sequence

Due to the varying adjustment ranges required for each strut, the moving platform experiences relatively large offsets after adjusting certain struts. After optimization, both the offset generated in each adjustment and the number of intermediate points with significant offsets are reduced. The total offset distance caused by adjusting all six struts and the average offset distance generated by each strut adjustment are shown in Table 3. Using the proposed method, the offset of the moving platform in a single adjustment is reduced by approximately 26.63%.

Table 3. Comparison of offset distances before and after strut adjustment sequence optimization

Number of Adjustments	Total Offset per Adjustment (mm)		Mean Offset of a Single Strut Adjustment (mm)	
	Before Optimization	After Optimization	Before Optimization	After Optimization
0–1	24.749	12.295	4.125	2.049
1–2	14.291	12.929	2.382	2.155
2–3	14.247	13.037	2.374	2.173
3–4	18.617	12.931	3.103	2.155
4–5	12.716	12.124	2.119	2.021
5–6	13.169	11.544	2.195	1.924
6–7	17.693	12.323	2.949	2.054
7–8	24.701	13.284	4.117	2.214
8–9	17.225	14.094	2.878	2.349
9–10	8.822	7.405	1.47	1.234
Total offset	166.23	121.966	27.712	20.328

The correction process is illustrated in Figure 8. Based on the principle of distraction osteogenesis, bones gradually grow under the traction of the fixator. However, this growth process is highly uncertain and can be influenced by the patient's recovery condition. Therefore, regular monitoring is necessary during clinical treatment to track progress. In the simulation experiment, a sufficient bone growth space was reserved. Upon completing the correction, a 25 mm gap between the midpoints of the two bone segments was maintained.

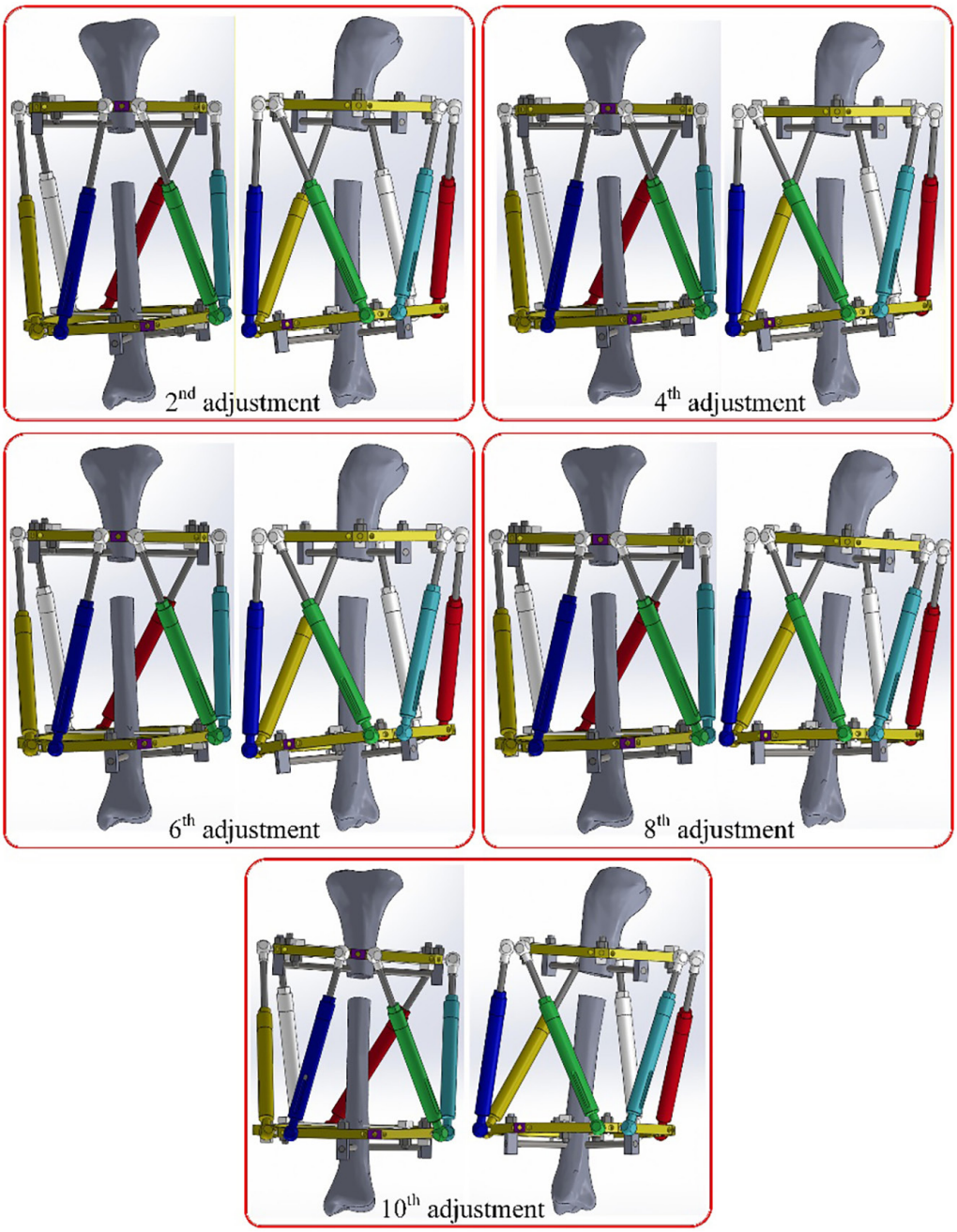

Fig. 8. Demonstration of the simulated orthopedic process

Upon the completion of the correction, the tibial deformity parameters were measured and are shown in Table 4. The results of the simulated experiments

demonstrate that the proposed method effectively provides the optimal adjustment lengths and sequence for the struts and achieves the goal of orthopedic correction.

Table 4. Deformity parameters upon completion of correction

Parameters	Values Before Correction
APD (mm)	17.76
LD (mm)	17.59
ALD_{ax} (mm)	25
APA (°)	0.15
LA (°)	0.22
APA_{ax} (°)	0

3.3 Clinical orthopedic assistance

Based on the results of the simulation experiment, the proposed method effectively corrected post-osteotomy tibial deformity. Typically, the formulation of orthopedic correction plans relies heavily on the clinical experience of orthopedic surgeons. Surgeons tailor the plans according to each patient's physical condition and age [11, 12]. Therefore, the surgeons' subjective judgment significantly influences the quality of the procedure. With the proposed assistance, surgeons still leaded the correction process. This study provided optimized adjustment plans to the surgeon based on follow-up observations, keeping the correction progress under their control. Since bone growth rate is unpredictable and the patient's daily activities may affect the correction outcome, follow-up observations were conducted every two months to monitor the progress. The proposed method dynamically generated updated plans based on the recovery status, enabling gradual adjustments of each strut to the specified node positions. The follow-up results are shown in Figure 9.

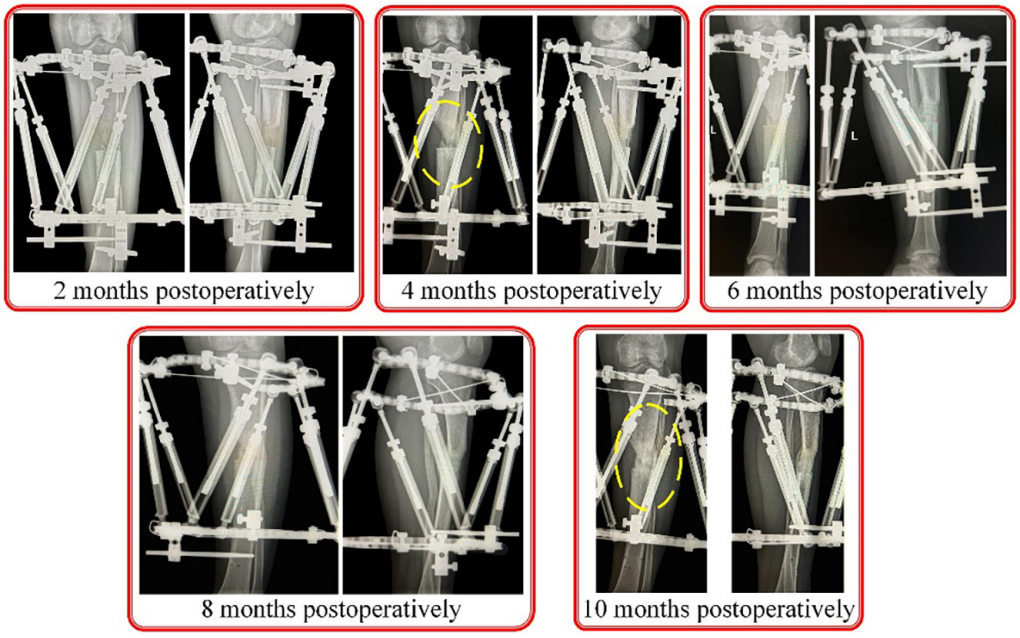

Fig. 9. Follow-up X-ray images

The process of frame traction and bone growth occurred simultaneously during the correction process. Significant bone growth was observed four months after surgery, as indicated by the yellow circle in Figure 9. By the 10th month of correction, the newly formed bone had fully fused with the distal segment. On the coronal plane, the anatomical axes of the proximal and distal segments were nearly aligned, effectively correcting the tibial deformity. Radiographic examination was performed, and the postoperative deformity parameters at 10 months are shown in Table 5.

Table 5. Deformity parameters at 10 months post-surgery

Parameters	Values Before Correction
APD (mm)	0
LD (mm)	0
APA (°)	0.864
LA (°)	5.692

4 CONCLUSION

As an advanced external fixator, the TSF enables simultaneous multi-plane corrections, yet its nonlinear coupling often leads to unintended platform deviations. To enhance patient comfort and correction smoothness, this study integrated TSF motion analysis with MOGA and ACO algorithms to optimize both the adjustment lengths and sequences of the struts. By minimizing intermediate platform offsets, the proposed method provides an algorithmically optimized plan that moves beyond conventional manual estimation or uniform length changes.

Physical experiments and a clinical feasibility demonstration confirmed that the method effectively achieves precise bone alignment while reducing unintended deviations. While larger step sizes were used in simulations to visualize deviation patterns, the algorithm remains fully compatible and valid under clinically realistic adjustment resolutions. Although results from this single case serve primarily as a proof-of-concept, the shift from manual estimation to optimized trajectory planning offers a personalized approach to deformity correction. This transition could significantly reduce the learning curve for surgeons and enhance the standard of care for complex limb reconstructions.

5 ACKNOWLEDGMENT

We thank Jiangsu Province Hospital in Nanjing, China, for providing valuable data.

This work was supported by the Key Talent Program of the Xinjiang Uygur Autonomous Region (No. 2024TSYCJC0029), the National Natural Science Foundation of China (Regional Project, No. 62366054), and the Scientific Research Start-up Fund Project of Yili Normal University (2025RCYJ54).

6 REFERENCES

[1] Y. Manggala, C. Angthong, and A. Primadhi, "The deformity correction and fixator-assisted treatment using Ilizarov versus Taylor spatial frame in the foot and ankle," *Orthopedic Reviews*, vol. 9, no. 4, p. 7337, 2017. https://doi.org/10.4081/or.2017.7337

[2] J. Messner, H. Chhina, and S. Davidson, "Clinical outcomes in pediatric tibial lengthening and deformity correction: A comparison of the Taylor Spatial Frame with the Orthex Hexapod System," *Journal of Childrens Orthopaedics*, vol. 15, no. 2, pp. 114–121, 2021. https://doi.org/10.1302/1863-2548.15.200165

[3] Y. S. Liu, F. Y. Cai, and K. Liu, "Intraoperative acute correction versus postoperative gradual correction for tibial shaft fractures with multiplanar posttraumatic deformities using the hexapod external fixator," *BMC Musculoskeletal Disorders*, vol. 22, no. 1, p. 8, 2021. https://doi.org/10.1186/s12891-021-04505-0

[4] A. V. Gubin, D. Y. Borzunov, and L. O. Marchenkova, "Contribution of G.A. Ilizarov to bone reconstruction: Historical achievements and state of the art," *Strategies in Trauma and Limb Reconstruction*, vol. 11, no. 3, pp. 145–152, 2016. https://doi.org/10.1007/s11751-016-0261-7

[5] N. Karamanis, A. T. Kermanidis, and L. A. Spyrou, "Taylor spatial frame behavior in high tibial osteotomies: A clinical-mechanical study," *Applied Sciences-Basel*, vol. 13, no. 6, p. 12, 2023. https://doi.org/10.3390/app13063837

[6] T. Liu, Y. H. Lu, and Y. Zhu, "Study on orthopaedic path planning of Taylor spatial frame," *International Journal of Medical Robotics and Computer Assisted Surgery*, vol. 20, no. 1, p. 14, 2024. https://doi.org/10.1002/rcs.2606

[7] X. P. Zhang, Y. S. Liu, and X. L. Ma, "The application of computer-assisted design in the reduction of long bone fractures with Taylor spatial frame," *Chinese Journal of Surgery*, vol. 56, no. 10, pp. 786–792, 2018. https://doi.org/10.3760/cma.j.issn.0529-5815.2018.10.017

[8] L. Zak, T. M. Tiefenboeck, and G. E. Wozasek, "Computed tomography in limb salvage and deformity correction—3D assessment, indications, radiation exposure, and safety considerations," *Journal of Clinical Medicine*, vol. 10, no. 17, p. 14, 2021. https://doi.org/10.3390/jcm10173781

[9] Y. S. Liu, H. Li, and J. L. Liu, "Long bone fracture reduction and deformity correction using the hexapod external fixator with a new method: A feasible study and preliminary results," *BMC Musculoskeletal Disorders*, vol. 22, no. 1, p. 8, 2021. https://doi.org/10.1186/s12891-021-04097-9

[10] S. D. Liu, Y. M. Song, and B. B. Lian, "A general pose recognition method and its accuracy analysis for 6-axis external fixation mechanism using image markers," *Machines*, vol. 10, no. 12, p. 17, 2022. https://doi.org/10.3390/machines10121234

[11] J. Gessmann, S. Frieler, and M. Königshausen, "Accuracy of radiographic measurement techniques for the Taylor spatial frame mounting parameters," *BMC Musculoskeletal Disorders*, vol. 22, no. 1, p. 7, 2021. https://doi.org/10.1186/s12891-021-04084-0

[12] K. Uko-Karcz, P. Kaptocz, and O. Hajnus, "Ilizarov technique: Innovations and applications in orthopedic surgery and bone reconstruction," *Medical Science Pulse*, vol. 19, no. 3, pp. 30–34, 2025. https://doi.org/10.5604/01.3001.0055.1948

7 AUTHORS

Tao Liu is a Lecturer at the College of Network Security and Information Technology, Yili Normal University, China. Research interests are in the fields of computer vision and medical image analysis (E-mail: liutao@ylnu.edu.cn).

Xiaolong Qi is an Associate Professor at the College of Network Security and Information Technology, Yili Normal University, China, and currently serves as the Vice Dean. Research interests are in the fields of causal learning and deep learning (E-mail: qixl@ylnu.edu.cn).

Yonghua Lu is a Professor at the College of Mechanical and Electrical Engineering, Nanjing University of Aeronautics & Astronautics. Research interests are in the fields of computer vision, artificial intelligence, visual recognition, multi-modal perception, and learning-based perception systems (E-mail: nuaa_lyh@nuaa.edu.cn).

Xinyu Di is a Ph.D. candidate at the College of Mechanical and Electrical Engineering, Nanjing University of Aeronautics and Astronautics, China. Research interests are in the fields of UAV object tracking and trajectory prediction (E-mail: dixinyu@nuaa.edu.cn).

Yu Zhang is a Deputy Chief Physician at the Department of Orthopedics, Jiangsu Province Hospital. Research interests are in the fields of trauma orthopedics and ankle surgery (E-mail: 893636863@qq.com).